# Close encounters between periodic light and periodic arrays of quantum emitters

Frieder Lindel, <sup>1,2,3</sup> Carlos J. Sánchez Martínez, <sup>1,2</sup> Johannes Feist, <sup>1,2,\*</sup> and Francisco J. García-Vidal<sup>1,2,†</sup>

<sup>1</sup>Departamento de Física Teórica de la Materia Condensada, Universidad Autónoma de Madrid, E-28049 Madrid, Spain 
<sup>2</sup>Condensed Matter Physics Center (IFIMAC), Universidad Autónoma de Madrid, E-28049 Madrid, Spain 
<sup>3</sup>Institute for Theoretical Physics, ETH Zürich, CH-8093 Zürich, Switzerland 
(Dated: August 4, 2025)

Periodically structured surfaces (metasurfaces), i.e., *periodic light*, have evolved as a powerful tool for manipulating electromagnetic fields both in classical and quantum regimes. However, no general approach for quantizing the electromagnetic fields and treating quantum light-matter interactions in such structures exists. Here, we construct an ab initio few-mode quantization scheme for metasurface resonances based on macroscopic quantum electrodynamics. We use our approach to propose a framework for strong light-matter coupling in which collective excitations of periodic arrays of quantum emitters are strongly coupled to the light modes supported by the metasurface, leading to the formation of *crystal polaritons*. As a proof-of-principle example of their potential, we show that interactions between crystal polaritons can lead to an efficient and directional generation of entangled photon pairs.

Confining photons in cavities can lead to strong coupling of single or few photonic modes to quantum emitters. This is at the heart of cavity quantum electrodynamics (QED), which has found a wide range of applications, such as the generation of non-classical states of light [1], quantum sensors [2], or in quantum information science [3]. Platforms for strong light-matter coupling include wavelength-sized cavities, whose coupling strengths are limited by the diffraction limit. Alternatively, light confinement via plasmonic nanoparticles or surface resonances [4–6] can lead to much higher light-matter coupling strengths; however, they suffer losses that limit their use for many applications in quantum optics.

A very successful platform in classical electrodynamics is provided by two-dimensional periodically structured surfaces (metasurfaces), which consist of metamaterials [7] or photonic crystals [8]. They are a well-established tool to manipulate classical light and offer many exciting design possibilities to support flat bands [9], topologically protected states [10, 11] and lasing [12–14], or bound states in the continuum [15–18]. More recently, they have been used to control quantum states of light as well [19, 20].

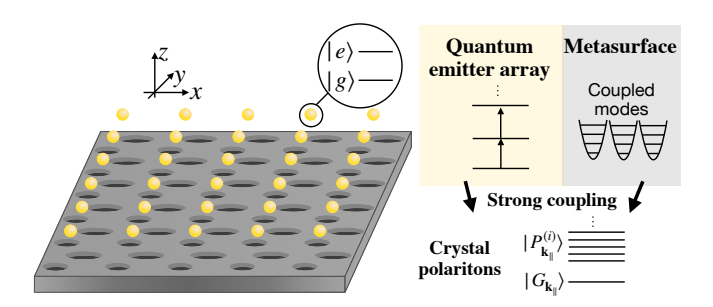


FIG. 1. Setup of the proposed cavity QED platform. A metasurface confines the light field in its vicinity that is strongly coupled to collective excitations of a quantum emitter array. Strong coupling of the quantized modes of the metasurface to the emitter array excitations leads to the formation of crystal polaritons.

Metasurfaces support photonic modes that have strong subwavelength field confinement, whereas losses are mitigated through the collective nature of the modes extending over many unit cells [21]. For example, collective strong coupling with surface lattice resonances has been demonstrated [22], and recent results report the onset of singleemitter strong coupling [23]. The former has been used further for polariton lasing [24, 25], polariton BECs [26] and polaritonic chemistry [27]. From the theoretical side, the field quantization of metasurfaces has so far only been considered for surface lattice resonances, treated within the coupled dipole approximation and linear response [28]. So, despite the versatility of metasurfaces and their potential for quantum applications, there exists no ab initio framework that can accurately determine the quantized resonant modes of metasurfaces to which nearby emitters couple.

On the other hand, arrays of quantum emitters in free space, such as arrays of cold atoms or molecules, typically considered for quantum simulations [29], have recently gained further interest due to their unique optical properties [30]. They offer great potential for classical optics [30–32], nonlinear quantum optics [33–37], or quantum information processing [38, 39]. Even when placed in close proximity to structured optical environments, their analysis has been limited to the weak-coupling regime, in which the electromagnetic field that mediates the interaction can be traced out [4, 40].

Here, we discuss the possibilities unlocked by strongly coupling emitter arrays to resonances of metasurfaces resulting in a polaritonic quantum metasurface, see Fig. 1. We first identify the coupled, lossy photonic modes of general metasurfaces to which collective excitations of emitter arrays couple. We account for material losses, dispersion, free-space emission, and retardation. As a result, we obtain a cavity QED-type Hamiltonian for this quantum optics platform, giving full access to the quantum dynamics in the strong-coupling regime. This allows us to quantify the coupling regime achievable with different platforms. We

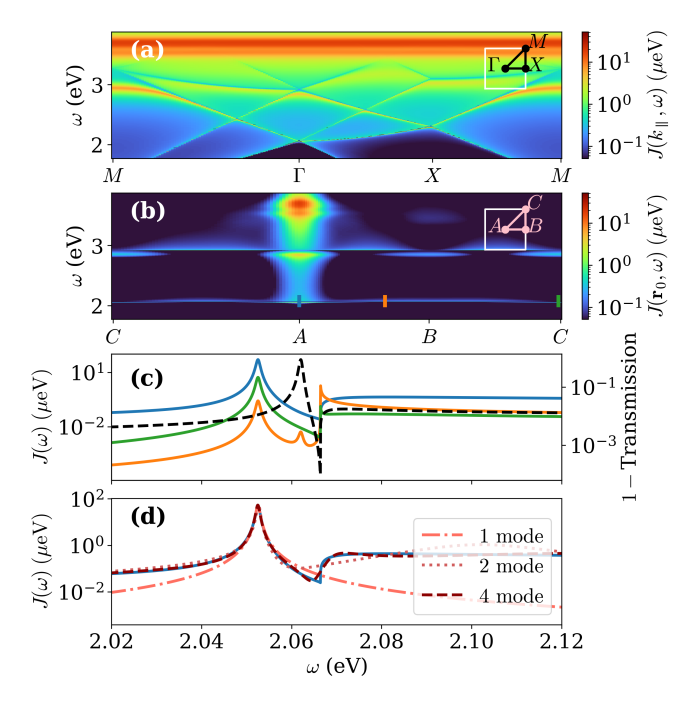


FIG. 2. Reciprocal-space spectral density J of a square array of silver nanospheres. (a) J as a function of frequency and inplane wave-vector along a path in reciprocal space as indicated by the inset for an emitter array positioned in the center of the unit cell [ $\mathbf{r}_{\parallel} = (0,0)$ ] and 10 nm above the nanospheres with dipole moment  $d=10\,\mathrm{D}$  and orientation  $\mathbf{n}=\mathbf{e}_z$ . (b) J at the  $\Gamma$  point ( $\mathbf{k}_{\parallel}=\mathbf{0}$ ) for different emitter positions [A:  $\mathbf{r}_{\parallel}=(0,0)$ , B:  $\mathbf{r}_{\parallel}=(300,0)\mathrm{nm}$ , C:  $\mathbf{r}_{\parallel}=(300,300)\mathrm{nm}$ ]. (c) Cut through J in (b) at three different positions indicated by vertical lines in (b) (colored lines) and the transmission through the array (black dashed line). (d) J for an emitter at A and the  $\Gamma$  point shown in (c) together with the fitted model spectral density  $J_{\mathrm{mod}}$  [Eq. (3)] with different numbers of modes.

find that strong coupling of emitter arrays with just a single emitter per unit cell to metallic nanoparticle arrays is hampered by plasmonic losses. In contrast, considering a bound state in the continuum of a *dielectric* nanoparticle array, strong coupling is achievable with state-of-the-art quantum emitters. This results in the hybridization of spin-wave excitations of the emitter array and metasurface resonances into what we will name crystal polaritons, which can be used for efficient (resonant) quantum light generation.

Reciprocal-space spectral density. The coupling of a single emitter to a resonator is determined by the spectral density evaluated at the position of the emitter [41, 42], in which cavity resonances appear as peaks [43, 44]. Accounting for dispersion and absorption, the spectral density can be obtained via macroscopic quantum electrodynamics in terms of the imaginary part of the dyadic Green tensor **G** [45, 46].

A similar strategy can be followed for periodic metasurfaces. To identify the extended modes of metasurfaces, we replace the localized emitters by arrays of two-level emit-

ters that share the same periodicity as the metasurface (for a straightforward extension to multilevel emitters see the Supplemental Material (SM) [47]). The emitters are characterized by their dipole operator  $\hat{d}_i^{(h)} = d_i(\hat{\sigma}_i^{(h)} + \hat{\sigma}_i^{(h)\dagger})$  and orientation  $\mathbf{n}^{(h)}$ , as well as their position  $\mathbf{r}_i^{(h)} = \mathbf{r}_0^{(h)} + \mathbf{R}_i$ , with  $\mathbf{r}_0^{(h)}$  denoting the position of the hth dipole in the reference unit cell and  $\{\mathbf{R}_i\}$  being the set of lattice vectors connecting the different unit cells. As we derive in the SM [47], the Bloch-periodic spin-wave excitations of such emitter arrays  $\hat{d}_{\mathbf{k}_{\parallel}}^{(h)} = \sum_i \hat{d}_i^{(h)} \mathrm{e}^{-i\mathbf{k}_{\parallel}\cdot\mathbf{r}_i^{(h)}}$  couple to the continuum of field modes via the reciprocal-space spectral density of the metasurface

$$J_{h,h'}(\mathbf{k}_{\parallel},\omega) = \frac{\mu_0 \omega^2}{\pi \hbar} d_h d_{h'} e^{-i\mathbf{k}_{\parallel}(r_0^{(h)} - r_0^{(h')})} \times \mathbf{n}^{(h)} \cdot \mathcal{G}_{\text{AH}}(\mathbf{k}_{\parallel}, \mathbf{r}_0^{(h)}, \mathbf{r}_0^{(h')}, \omega) \cdot \mathbf{n}^{(h')}. \quad (1)$$

Here,  $\mathcal{G}_{\mathrm{AH}}$  is the anti-Hermitian part of the Bloch-periodic Green tensor  $\mathcal{G}(\mathbf{k}_{\parallel},\mathbf{r},\mathbf{r}',\omega)=\sum_{i}\mathrm{e}^{\mathrm{i}\mathbf{k}_{\parallel}\cdot\mathbf{R}_{i}}\mathbf{G}(\mathbf{r},\mathbf{r}'+\mathbf{R}_{i},\omega)$  [48, 49].

We have thus identified  $J_{h,h'}(\mathbf{k}_{\parallel},\omega)$  as the crucial quantity that fully determines the optical environment of the metasurface seen by the emitter array and thus characterizes the extended resonances of metasurfaces. To illustrate this quantity, we consider a square array of silver nanospheres with radius R=50 nm and lattice constant a=600 nm that is coupled to an array of two-level emitters with a single emitter per unit cell located at different positions within the unit cell. The dipole moment of the two-level emitters is given by d=10 D and the response of the silver spheres is described by a Drude permittivity as in Ref. [50].

As shown in Fig. 2, the maxima of the reciprocal-space spectral density  $J \equiv J_{1,1}(\mathbf{k}_{\parallel},\omega)$  follow the usual dispersion of the surface lattice resonances of the plasmonic array, resulting from the coupling of diffractive orders (Rayleigh anomalies) with the plasmonic resonance of the nanoparticles (here at  $3.5\,\mathrm{eV}$ ) [51]. Although for certain emitter positions the dispersion of the maxima looks similar, the resonances in the reciprocal-space spectral density J differ qualitatively from physical magnitudes that have been used so far to identify the mode structure of metasurfaces [22, 52] such as the reflectance, transmittance or extinction of the array, see Fig. 2 (c). Furthermore, in contrast to these quantities, the optical environment felt by the emitter, encoded in J, depends on its orientation and position in the unit cell, the latter shown in Fig. 2 (b).

Few-mode quantization of metasurfaces. To gain further insight into the mode structure of metasurfaces and to enable the numerically efficient study of the strong coupling regime, we construct a few-mode model [53–58] in which the continuum of field modes seen by the emitters is equivalently described by a set of few coupled lossy field modes given by creation and annihilation operators  $\hat{a}_{\mathbf{k}_{\parallel},i}^{(\dagger)}$ . The density matrix  $\hat{\rho}$  of the emitters and the modes evolves as  $\hat{\rho} = 1/(V_B) \int\!\!\mathrm{d}^2k_{\parallel}(-\mathrm{i})[\hat{H}_{\mathbf{k}_{\parallel}},\hat{\rho}] + \sum_i \kappa_{\mathbf{k}_{\parallel},i} L_{\hat{a}_{\mathbf{k}_{\parallel},i}}[\hat{\rho}],$  with

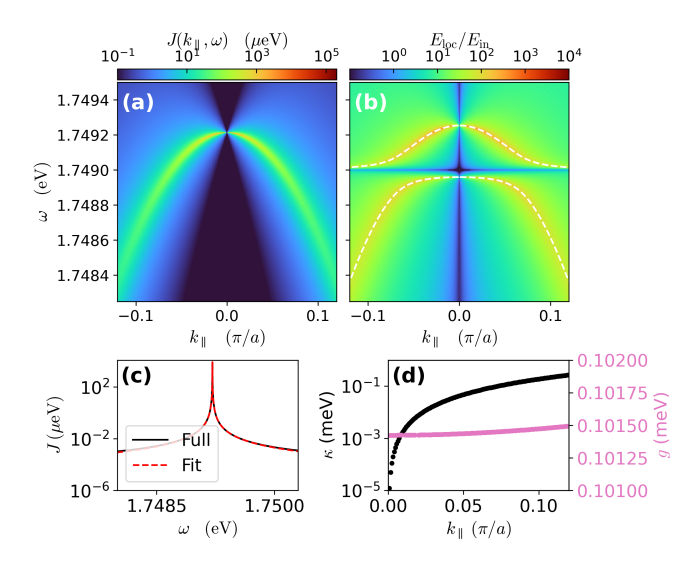


FIG. 3. Strong coupling to a bound state in the continuum. (a) Dispersion of the reciprocal-space spectral density J for a square array of dielectric (silicon) nanospheres with radius  $R=100\,\mathrm{nm}$ , refractive index n=3.5, lattice constant  $a=400\,\mathrm{nm}$ ,  $\mathbf{k}_{\parallel}=k_{\parallel}\mathbf{e}_{y}$ , and the emitter array is positioned at  $(0,105\,\mathrm{nm},0)$  in the unit cell with frequency  $\omega_E=1.749\,\mathrm{eV}$ , dipole moment  $d=10\,\mathrm{D}$ , and orientation  $\mathbf{n}=\mathbf{e}_x$ . (b) Local field strength  $E_{\mathrm{loc}}$  at the position of the emitter as a function of the frequency  $\omega_L$  and inplane momentum  $\mathbf{k}_L=k_L\mathbf{e}_y$  of the plane-wave laser driving with amplitude  $E_{\mathrm{in}}$  and polarization  $\mathbf{e}_x$ . (c) Exemplary single-mode fit of J at  $k_{\parallel}=6.4\times10^{-3}\pi/a$ . Coupling strength g and decay rate  $\kappa$  of the bound state in the continuum obtained from fitting a single-mode model to J at different in-plane momenta. The dispersion of the crystal polaritons is shown by the dashed lines in (b).

the Lindblad dissipator  $L_{\hat{O}}[\hat{\rho}]=\hat{O}\hat{\rho}\hat{O}^{\dagger}-\frac{1}{2}\{\hat{O}^{\dagger}\hat{O},\hat{\rho}\}$ , the Brillouin zone volume  $V_B$ , and the few-mode Hamiltonian ( $\hbar=1$ ):

$$\hat{H}_{\mathbf{k}_{\parallel}} = \hat{H}_{e,\mathbf{k}_{\parallel}} + \sum_{i,j} \omega_{\mathbf{k}_{\parallel},ij} \hat{a}^{\dagger}_{\mathbf{k}_{\parallel},i} \hat{a}_{\mathbf{k}_{\parallel},j} + \sum_{i,h} (g_{\mathbf{k}_{\parallel},ih} \hat{d}^{(h)\dagger}_{\mathbf{k}_{\parallel}} \hat{a}_{\mathbf{k}_{\parallel},i} + \text{h.c.}). \quad (2)$$

Here,  $\hat{H}_{e,\mathbf{k}_{\parallel}}$  is the bare emitter Hamiltonian. Equivalence between the few-mode model and the full multimode Hamiltonian is achieved by matching the reciprocal-space spectral density in Eq. (1) to the corresponding spectral density of the few-mode model

$$\mathbf{J}_{\text{mod}}(\mathbf{k}_{\parallel}, \omega) = \frac{1}{\pi} \mathbf{g}_{\mathbf{k}_{\parallel}} \cdot \operatorname{Im}\left[\frac{1}{\widetilde{\mathbf{H}}_{\mathbf{k}_{\parallel}} - \omega}\right] \cdot \mathbf{g}_{\mathbf{k}_{\parallel}}^{\dagger}, \quad (3)$$

with  $\widetilde{H}_{\mathbf{k}_{\parallel},ij} = \omega_{\mathbf{k}_{\parallel},ij} - \mathrm{i}\kappa_{\mathbf{k}_{\parallel},i}\delta_{ij}/2$ . This can be achieved by fitting the parameters of the few-mode model, namely the mode frequencies  $\omega_{\mathbf{k}_{\parallel},ii}$ , the mode couplings  $\omega_{\mathbf{k}_{\parallel},ij}$ , and the decay rates  $\kappa_{\mathbf{k}_{\parallel},i}$ , as well as the light-matter coupling constants  $g_{\mathbf{k}_{\parallel},ih}$ .

Applying this procedure to a representative surface lattice resonance in the plasmonic array considered above, we find that a single resonance generally requires more than one lossy photonic mode for an accurate description [see Fig. 2(d)]. This stems from the asymmetric lineshape observed in the reciprocal-space spectral density [59], in contrast to the symmetric Lorentzian expected for a single mode [cf. Eq. (3)]. Physically, the asymmetry—and hence the multimode nature—can be attributed to the inherent asymmetry of the Rayleigh anomalies. As a result, resonances associated with a single peak in the spectral density (or extinction) are typically composed of a set of *coupled* modes, rather than a single one, contrary to common assumptions in the literature.

Polaritonic quantum metasurface. We have thus derived a way to identify the quantized mode structure of general periodic optical environments. We proceed by analyzing the potential of strongly coupling arrays of quantum emitters to such surfaces to obtain a polaritonic quantum metasurface. All elements of this experimental setup can be achieved with state-of-the-art devices. The main experimental challenge is to place the emitters in an array with fixed relative position to the nanoparticle. Promising platforms to do so are carbon-based color centers in hexagonal boron nitride films [23, 60], atoms trapped by Casimir–Polder forces of the metasurface [61, 62], or molecules placed via DNA origami [63, 64].

For the plasmonic array considered above, we obtain the cavity QED parameters of the quantized surface lattice resonances from the fit of the few-mode model. We find that with a single emitter per unit cell that has a dipole moment of  $10\,\mathrm{D}$ , the setup is close but does not quite reach the strong-coupling regime. As will be discussed elsewhere, the strong-coupling regime might be reached with plasmonic arrays using larger lattice constants, and it will be reached via collective strong coupling with several emitters per unit cell, in which case we expect quantum effects to be less pronounced.

As a second example, we consider a square array of dielectric (silicon) nanospheres. We focus on a bound state in the continuum (BIC) originating from the magnetic dipole resonance of the spheres [65], compare Fig. 3(a). We identify the BIC as an approximately Lorentzian resonance in the reciprocal-space spectral density, whose width decreases with decreasing in-plane wave vector. The BIC resonance is much sharper compared to the resonances of the plasmonic array considered above, resulting in much smaller decay rates and allowing for strong coupling for a single emitter in the unit cell, as we will show below.

We find that the Lorentzian BIC resonance in the reciprocal-space spectral density can be modeled by a single lossy mode for each value of the in-plane wave-vector, see Fig. 3 (c). We further obtain the decay rate and coupling strength of this mode to an emitter with a dipole moment of  $10\,\mathrm{D}$  and a frequency of  $\omega_E=1.749\,\mathrm{eV}$  via a single-mode fit and show them as a function of in-plane momentum in Fig. 3 (d). While the decay rate vanishes when approach-

ing the  $\Gamma$  point at  $\mathbf{k}_{\parallel}=\mathbf{0}$ , leading to a divergent quality factor, we find that the coupling strength remains finite and essentially constant over the resolved wave-vector range. Clearly we find  $g>\kappa$ , such that we are in the strong coupling regime. To confirm this, we show the electric field at the position of the emitter under plane-wave driving with different in-plane momenta and frequencies in Fig. 3 (b). A clear anticrossing indicating the strong-coupling regime can be found. The dispersion of these polariton modes can be obtained by diagonalizing the single excitation manifold of the few-mode Hamiltonian [white dashed line in Fig. 3 (b)]. This offers a highly tuneable strong-coupling platform, as many different crystal polaritons can be realized depending on the lattice geometry and the position of the emitter.

Quantum light generation with the polaritonic quantum metasurface. One of the many applications of cavity-QED platforms is quantum light generation [1]. Here, we show that the proposed polaritonic quantum metasurface can efficiently generate directionally emitted, entangled photon pairs, with the tunable design of the metasurface allowing flexible control over the quantum properties of the photon pair.

We consider the same dielectric array of nanospheres and emitter array as before (see Fig. 3) driven by a laser with fixed frequency  $\omega_L$  and in-plane momentum  $\mathbf{k}_L$ . In the low-excitation regime, we can approximate the two-level emitters by harmonic oscillators with annihilation operators  $\hat{b}_{\mathbf{k}_{\parallel}}$ . As a result,  $\mathbf{k}_{\parallel}$  is conserved and in the steady state the laser driving coherently displaces the modes and the

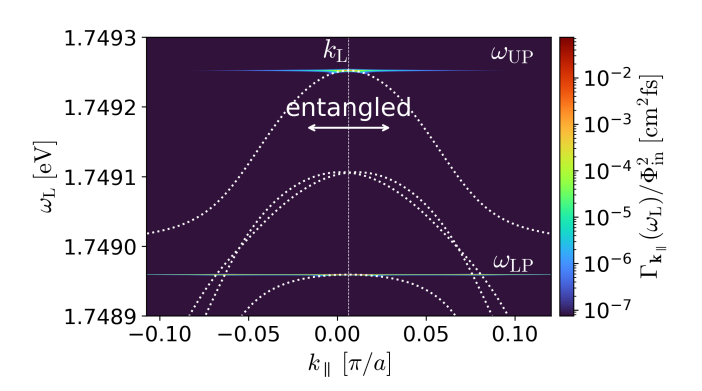


FIG. 4. Quantum light generation with the polaritonic quantum metasurface. Two-photon emission rate density  $\Gamma_{\mathbf{k}_{\parallel}}$  normalized by the incoming flux density  $\Phi_{\mathrm{in}}^2$  ( $\Gamma_{\mathbf{k}_{\parallel}} \propto \Phi_{\mathrm{in}}^2$  in the perturbative regime) for  $k_{\mathrm{L}} = 6.4 \times 10^{-3} \pi/a$  (vertical dotted line) and  $V_d/V_B = 1.6 \times 10^{-5}$  as a function of laser frequency  $\omega_L$  and in-plane momentum  $\mathbf{k}_{\parallel} = k_{\parallel} \mathbf{e}_y$  of one of the emitted photons (in-plane momentum of the other emitted photon is fixed to  $2k_{\mathrm{L}} - k_{\parallel}$  such that the plot is symmetric around  $k_{\mathrm{L}}$ ). Enhanced two-photon emission occurs when the laser frequency is in resonance with the upper or lower crystal polaritons at the laser momentum  $\omega_{\mathrm{UP}/\mathrm{LP}}$  and the resonance condition  $\omega(\mathbf{k}_{\parallel}) + \omega(\overline{\mathbf{k}}_{\parallel}) = 2\omega_L$ , shown by white dashed lines, is satisfied.

emitters with momentum  $\mathbf{k}_L$  by  $a_{\mathbf{k}_L,i}$  and  $b_{\mathbf{k}_L}$ , respectively, while all emitter and photon states with  $\mathbf{k}_{\parallel} \neq \mathbf{k}_L$  remain in the ground state.

Next, we introduce the nonlinearity of the two-level emitters via the next–order Holstein–Primakoff expansion [66, 67] of  $\hat{\sigma}_{\mathbf{k}_{\parallel}}$  in terms of  $\hat{b}_{\mathbf{k}_{\parallel}}$ . Assuming that the nonlinearity is weak, we find the lowest-order correction affecting modes with  $\mathbf{k}_{\parallel} \neq \mathbf{k}_{\rm L}$  to be given by a squeezing and a beam-splitter contribution, see SM [47]. The beam-splitter contribution leads to a negligible shift of the mode and emitter frequencies, while the squeezing Hamiltonian leads to the generation of entangled excitations and reads

$$\begin{split} \hat{H}_{\mathrm{sq},\mathbf{k}_{\parallel}} &= \sum_{i} g_{\mathbf{k}_{\parallel},i}^{*} \beta_{\mathbf{k}_{\perp}}^{2} \hat{a}_{\mathbf{k}_{\parallel},i}^{\dagger} \hat{b}_{\overline{\mathbf{k}}_{\parallel}}^{\dagger} \\ &+ E_{\mathrm{loc}} \delta_{\mathbf{k}_{\perp}} \hat{b}_{\mathbf{k}_{\parallel}}^{\dagger} \hat{b}_{\overline{\mathbf{k}}_{\parallel}}^{\dagger} + (\mathbf{k}_{\parallel} \leftrightarrow \overline{\mathbf{k}}_{\parallel}) + \mathrm{h.c.}, \end{split}$$
(4)

where  $(\mathbf{k}_{\parallel} \leftrightarrow \overline{\mathbf{k}}_{\parallel})$  denotes adding the preceding terms subject to the replacement  $\mathbf{k}_{\parallel} \leftrightarrow \overline{\mathbf{k}}_{\parallel}$  with  $\overline{\mathbf{k}}_{\parallel} \equiv 2\mathbf{k}_{\rm L} - \mathbf{k}_{\parallel}$ . Allowing for up to two excitations in the system, we can numerically identify the steady-state two-photon emission rate at a fixed wavevector  $\mathbf{k}_{\parallel}$  defined by  $\gamma_{\mathbf{k}_{\parallel}} = \sum_{i,j} (\kappa_{\mathbf{k}_{\parallel},i} + \kappa_{\overline{\mathbf{k}}_{\parallel},j}) \langle \hat{a}^{\dagger}_{\mathbf{k}_{\parallel},i} \hat{a}^{\dagger}_{\overline{\mathbf{k}}_{\parallel},i} \hat{a}_{\overline{\mathbf{k}}_{\parallel},i} \hat{a}_{\overline{\mathbf{k}}_{\parallel},j} \rangle_{\rm ss}$ . Here,  $\langle \dots \rangle_{\rm ss}$  is the steady-state expectation value. The two-photon emission rate density per unit area into a certain range of wave-vectors  $\mathbf{k}_{\parallel} \in V_d$  is defined by  $\Gamma_{\mathbf{k}_{\parallel}} = 1/(4\pi^2) \int_{V_d} \mathrm{d}^2 k_{\parallel} \gamma_{\mathbf{k}_{\parallel}}$  and can be approximated by  $\Gamma_{\mathbf{k}_{\parallel}} = V_d/(4\pi^2) \gamma_{\mathbf{k}_{\parallel}}$  for small  $V_d$ . Note that since the Hamiltonian in Eq. (4) always generates pairs of excitations at  $\mathbf{k}_{\parallel}$  and  $\overline{\mathbf{k}}_{\parallel}$ , the emitted photons are strongly entangled and we only have to integrate over a single wave-vector  $\mathbf{k}_{\parallel}$ , while the wave-vector of the other emitted photon is fixed by momentum conservation to  $2\mathbf{k}_{\rm L} - \mathbf{k}_{\parallel}$ .

In Fig. 4, we plot  $\Gamma_{\mathbf{k}_{\parallel}}$  for  $k_L = 6.4 \times 10^{-3} \pi/a$  as a function of the laser driving frequency  $\omega_L$  and the in-plane momentum of one of the emitted photons  $k_{\parallel}$ . The maxima in the two-photon emission rates can be understood as a result of two resonant conditions: (i) the laser driving has to be resonant with one of the polaritonic modes  $\omega_{\mathrm{UP}}$  and  $\omega_{\rm LP}$  at  ${\bf k}_L$  (the maxima in Fig. 4 (a) are clearly centered around  $\omega_{\rm UP}$  and  $\omega_{\rm LP}$ ); (ii) and momentum (phase-matching) and energy must be conserved, i.e. there must be polaritonic modes with frequencies  $\omega(\mathbf{k}_{\parallel})$  and  $\omega(\mathbf{k}_{\parallel})$  satisfying  $\omega(\mathbf{k}_{\parallel}) + \omega(\overline{\mathbf{k}}_{\parallel}) = 2\omega_L$ . These conditions are plotted by the white dashed lines in Fig. 4. As a result of both resonant conditions, we see maxima in the two-photon emission rate when the dashed lines cross  $\omega_{\rm LP}$  or  $\omega_{\rm UP}$  in Fig. 4. We find that the normalized two-photon emission rate  $\Gamma_{{f k}_{\parallel}}/\Phi_{
m in}^2$ emitted into a narrow fraction  $V_d/V_{\rm B}=1.6\times 10^{-5}$  of the Birllouin zone  $V_B$  can reach values up to  $10^{-2}$  cm<sup>2</sup>fs. This means that for an incoming laser power density of, e.g., just  $P = 10 \,\mu\text{W}/\text{cm}^2$  the conversion efficiency into that narrow range of wave-vectors is  $\Gamma_{\mathbf{k}_{\parallel}}/\Phi_{\mathrm{in}}=3.6\times10^{-4}$ and for  $P > 28 \text{mW/cm}^2$  the system would already be

far in the non-perturbative regime (perturbative conversion efficiency > 1). Note that the photonic component of the generated crystal polaritons leads to efficient out-coupling of the excitation to free space before the emitters can lose the excitation nonradiatively.

Conclusion and outlook. We have developed a theoretical model that identifies the quantized modes of metasurfaces accounting for dispersion, absorption, and general array geometries. Building on this, we further introduced a cavity QED platform in which collective excitations of emitter arrays are coupled to the modes of metasurfaces and discussed the possibility of reaching the strong-coupling regime with just a single emitter in the unit cell. We illustrated its use for quantum optics with the example of quantum light generation. The complete setup can be seen as a polaritonic quantum metasurface with many different design possibilities and, thus, different possible future research directions of this platform. We have here focused on wavelength-sized arrays, but sub-wavelength arrays are also expected to reach the strong-coupling regime and offer great potential for quantum optics [30-40]. Moreover, chiral electromagnetic modes, whose design in typical cavity QED platforms is challenging and which are of particular interest in chiral sensing and nonreciprocal quantum devices, as well as topologically nontrivial states of finite-sized metasurfaces, could be harnessed in the future by the proposed polaritonic quantum metasurface.

We acknowledge financial support by the Spanish Ministerio de Ciencia y Universidades—Agencia Estatal de Investigación through grants PID2021-125894NB-I00, EUR2023-143478, and CEX2023-001316-M through the María de Maeztu program for Units of Excellence in R&D, and from the European Union's Horizon Europe research and innovation programme under Grant Agreements No. 101070700 (MIRAQLS) and No. 101098813 (SCOLED). The work was further supported by the ETH Quantum Center Research Fellowship and the Dr Alfred and Flora Spälti Fonds.

- \* johannes.feist@uam.es
- † fj.garcia@uam.es
- [1] S. Haroche and J.-M. Raimond, *Exploring the quantum: atoms, cavities, and photons* (Oxford University Press, Oxford, 2006).
- [2] C. L. Degen, F. Reinhard, and P. Cappellaro, Rev. Mod. Phys. 89, 035002 (2017).
- [3] H. J. Kimble, Nature 453, 1023 (2008).
- [4] D. Chang, J. Douglas, A. González-Tudela, C.-L. Hung, and H. Kimble, Rev. Mod. Phys. **90**, 031002 (2018).
- [5] J. Fregoni, F. J. Garcia-Vidal, and J. Feist, ACS Photonics 9, 1096 (2022).
- [6] A. González-Tudela, A. Reiserer, J. J. García-Ripoll, and F. J. García-Vidal, Nat. Rev. Phys. 6, 166 (2024).
- [7] V. M. Shalaev, Nat. Photon. 1, 41 (2007).

- [8] J. D. Joannopoulos, P. R. Villeneuve, and S. Fan, Solid State Commun. 102, 165 (1997).
- [9] S. Mukherjee, A. Spracklen, D. Choudhury, N. Goldman, P. Öhberg, E. Andersson, and R. R. Thomson, Phys. Rev. Lett. 114, 245504 (2015).
- [10] L. Lu, C. Fang, L. Fu, S. G. Johnson, J. D. Joannopoulos, and M. Soljačić, Nat. Phys. 12, 337 (2016).
- [11] X. Ni, S. Yves, A. Krasnok, and A. Alu, Chem. Rev. 123, 7585 (2023).
- [12] B. Bahari, A. Ndao, F. Vallini, A. El Amili, Y. Fainman, and B. Kanté, Science 358, 636 (2017).
- [13] M. A. Bandres, S. Wittek, G. Harari, M. Parto, J. Ren, M. Segev, D. N. Christodoulides, and M. Khajavikhan, Science 359, eaar4005 (2018).
- [14] C. Han, M. Kang, and H. Jeon, ACS Photonics 7, 2027 (2020).
- [15] S. Fan and J. D. Joannopoulos, Phys. Rev. B 65, 235112 (2002).
- [16] Y. Plotnik, O. Peleg, F. Dreisow, M. Heinrich, S. Nolte, A. Szameit, and M. Segev, Phys. Rev. Lett. 107, 183901 (2011).
- [17] C. W. Hsu, B. Zhen, J. Lee, S.-L. Chua, S. G. Johnson, J. D. Joannopoulos, and M. Soljačić, Nature 499, 188 (2013).
- [18] C. W. Hsu, B. Zhen, A. D. Stone, J. D. Joannopoulos, and M. Soljačić, Nat. Rev. Mat. 1, 1 (2016).
- [19] T. Santiago-Cruz, S. D. Gennaro, O. Mitrofanov, S. Addamane, J. Reno, I. Brener, and M. V. Chekhova, Science 377, 991 (2022).
- [20] A. S. Solntsev, G. S. Agarwal, and Y. S. Kivshar, Nat. Photon. 15, 327 (2021).
- [21] S. Zou, N. Janel, and G. C. Schatz, J. Chem. Phys. 120, 10871 (2004).
- [22] A. I. Väkeväinen, R. J. Moerland, H. T. Rekola, A.-P. Eskelinen, J.-P. Martikainen, D.-H. Kim, and P. Törmä, Nano Letters 14, 1721 (2014).
- [23] T. T. H. Do, M. Nonahal, C. Li, V. Valuckas, H. H. Tan, A. I. Kuznetsov, H. S. Nguyen, I. Aharonovich, and S. T. Ha, Nat. Commun. 15, 2281 (2024).
- [24] M. Ramezani, A. Halpin, A. I. Fernández-Domínguez, J. Feist, S. R.-K. Rodriguez, F. J. Garcia-Vidal, and J. Gómez Rivas, Optica 4, 31 (2016).
- [25] A. I. Väkeväinen, A. J. Moilanen, M. Nečada, T. K. Hakala, K. S. Daskalakis, and P. Törmä, Nat. Commun. 11, 3139 (2020).
- [26] T. K. Hakala, A. J. Moilanen, A. I. Väkeväinen, R. Guo, J.-P. Martikainen, K. S. Daskalakis, H. T. Rekola, A. Julku, and P. Törmä, Nat. Phys. 14, 739 (2018).
- [27] F. Verdelli, Y.-C. Wei, K. Joseph, M. S. Abdelkhalik, M. Goudarzi, S. H. Askes, A. Baldi, E. Meijer, and J. Gomez Rivas, Angew. Chem. Int. Ed. 63, e202409528 (2024).
- [28] M. Reitz, S. v. d. Wildenberg, A. Koner, G. C. Schatz, and J. Yuen-Zhou, arXiv preprint arXiv:2502.02836 (2025).
- [29] M. Morgado and S. Whitlock, AVS Quantum Sci. 3 (2021).
- [30] J. Rui, D. Wei, A. Rubio-Abadal, S. Hollerith, J. Zeiher, D. M. Stamper-Kurn, C. Gross, and I. Bloch, Nature 583, 369 (2020).
- [31] E. Shahmoon, D. S. Wild, M. D. Lukin, and S. F. Yelin, Phys. Rev. Lett. 118, 113601 (2017).
- [32] J. Perczel, J. Borregaard, D. E. Chang, H. Pichler, S. F. Yelin, P. Zoller, and M. D. Lukin, Phys. Rev. A 96, 063801 (2017).

- [33] R. J. Bettles, M. D. Lee, S. A. Gardiner, and J. Ruostekoski, Commun. Phys. 3, 141 (2020).
- [34] M. Moreno-Cardoner, D. Goncalves, and D. E. Chang, Phys. Rev. Lett. 127, 263602 (2021).
- [35] L. Zhang, V. Walther, K. Mølmer, and T. Pohl, Quantum 6, 674 (2022).
- [36] S. P. Pedersen, L. Zhang, and T. Pohl, Phys. Rev. Res. 5, L012047 (2023).
- [37] S. P. Pedersen, G. M. Bruun, and T. Pohl, Phys. Rev. Res. 6, 043264 (2024).
- [38] A. Asenjo-Garcia, M. Moreno-Cardoner, A. Albrecht, H. Kimble, and D. E. Chang, Phys. Rev. X 7, 031024 (2017).
- [39] D. Bluvstein, S. J. Evered, A. A. Geim, S. H. Li, H. Zhou, T. Manovitz, S. Ebadi, M. Cain, M. Kalinowski, D. Hangleiter, et al., Nature 626, 58 (2024).
- [40] M. Reitz, C. Sommer, and C. Genes, PRX Quantum 3, 010201 (2022).
- [41] H.-P. Breuer and F. Petruccione, *The theory of open quantum systems* (Oxford University Press, Oxford, 2002).
- [42] P. Menczel, K. Funo, M. Cirio, N. Lambert, and F. Nori, Phys. Rev. Res. 6, 033237 (2024).
- [43] A. Imamoğlu, Phys. Rev. A **50**, 3650 (1994).
- [44] S. Y. Buhmann and D.-G. Welsch, Phys. Rev. A 77, 012110 (2008).
- [45] S. Scheel and S. Buhmann, Acta Phys. Slovaca 58, 675 (2008).
- [46] J. Feist, A. I. Fernández-Domínguez, and F. J. García-Vidal, Nanophotonics 10, 477 (2020).
- [47] See Supplemental Material at [URL will be inserted by publisher] for further details.
- [48] R. E. Jorgenson and R. Mittra, IEEE Trans. Antennas Propag. 38, 633 (2002).
- [49] C. M. Linton, SIAM Rev. **52**, 630 (2010).
- [50] A. Delga, J. Feist, J. Bravo-Abad, and F. Garcia-Vidal, Phys. Rev. Lett. 112, 253601 (2014).
- [51] C. Cherqui, M. R. Bourgeois, D. Wang, and G. C. Schatz, Acc. Chem. Res. 52, 2548 (2019).
- [52] S. R. K. Rodriguez, A. Abass, B. Maes, O. T. Janssen, G. Vecchi, and J. Gómez Rivas, Phys. Rev. X 1, 021019 (2011).
- [53] D. Tamascelli, A. Smirne, S. F. Huelga, and M. B. Plenio, Phys. Rev. Lett. 120, 030402 (2018).
- [54] D. Lentrodt and J. Evers, Phys. Rev. X 10, 011008 (2020).
- [55] I. Medina, F. J. García-Vidal, A. I. Fernández-Domínguez, and J. Feist, Phys. Rev. Lett. 126, 093601 (2021).
- [56] M. Sánchez-Barquilla, F. J. García-Vidal, A. I. Fernández-Domínguez, and J. Feist, Nanophotonics 11, 4363 (2022).
- [57] C. J. Sánchez Martínez, J. Feist, and F. J. García-Vidal, Nanophotonics 13, 2669 (2024).
- [58] M. Lednev, D. Fernández de la Pradilla, F. Lindel, E. Moreno, F. J. García-Vidal, and J. Feist, PRX Quantum 6, 020361 (2025).
- [59] D. Lentrodt, O. Diekmann, C. H. Keitel, S. Rotter, and J. Evers, Phys. Rev. Lett. 130, 263602 (2023).
- [60] T. T. Tran, K. Bray, M. J. Ford, M. Toth, and I. Aharonovich, Nature Nanotechnol. 11, 37 (2016).
- [61] M. Gullans, T. Tiecke, D. Chang, J. Feist, J. Thompson, J. I. Cirac, P. Zoller, and M. D. Lukin, Phys. Rev. Lett. 109, 235309 (2012).
- [62] A. González-Tudela, C.-L. Hung, D. E. Chang, J. I. Cirac, and H. Kimble, Nat. Photonics 9, 320 (2015).

- [63] R. J. Kershner, L. D. Bozano, C. M. Micheel, A. M. Hung, A. R. Fornof, J. N. Cha, C. T. Rettner, M. Bersani, J. Frommer, P. W. Rothemund, et al., Nat. Nanotechnol. 4, 557 (2009).
- [64] A. Kuzyk, R. Jungmann, G. P. Acuna, and N. Liu, ACS Photonics 5, 1151 (2018).
- [65] D. R. Abujetas and J. A. Sánchez-Gil, Nanomaterials 11, 998 (2021).
- [66] T. Holstein and H. Primakoff, Phys. Rev. 58, 1098 (1940).
- [67] M. Vogl, P. Laurell, H. Zhang, S. Okamoto, and G. A. Fiete, Phys. Rev. Res. 2, 043243 (2020).

# **Supplemental Material**

(for the article: "Close encounters between periodic light and periodic arrays of quantum emitters")

### SI. LIGHT-MATTER INTERACTION IN 2D PERIODIC PHOTONIC STRUCTURES

A formal quantization of the electromagnetic field in arbitrary structures, including dispersive and lossy media, is achieved by the macroscopic QED formalism [1, 2]. This framework describes the electromagnetic field through a set of bosonic vector operators  $\{\hat{\mathbf{f}}_p(\mathbf{r},\omega)\}$  projected on the dyadic Green tensor  $\mathbf{G}(\mathbf{r},\mathbf{r}',\omega)$ . The electric field operator reads

$$\hat{\mathbf{E}}(\mathbf{r}) = \sum_{p=e,m} \int_0^\infty d\omega \int d^3r' \left[ \mathbf{G}_p(\mathbf{r}, \mathbf{r}', \omega) \cdot \hat{\mathbf{f}}_p(\mathbf{r}', \omega) + \text{h.c.} \right], \tag{S5}$$

where the amplitude coefficients  $\mathbf{G}_p(\mathbf{r},\mathbf{r}',\omega)$  are related to the dyadic Green tensor by

$$\mathbf{G}_{e}(\mathbf{r}, \mathbf{r}', \omega) = i \frac{\omega^{2}}{c^{2}} \sqrt{\frac{\hbar}{\pi \epsilon_{0}}} \operatorname{Im} \epsilon(\mathbf{r}', \omega) \mathbf{G}(\mathbf{r}, \mathbf{r}', \omega), \tag{S6}$$

$$\mathbf{G}_{m}(\mathbf{r}, \mathbf{r}', \omega) = i \frac{\omega}{c} \sqrt{\frac{\hbar}{\pi \epsilon_{0}} \frac{\operatorname{Im} \mu(\mathbf{r}', \omega)}{|\mu(\mathbf{r}', \omega)|^{2}}} \times \left[\overrightarrow{\nabla}_{r'} \times \mathbf{G}(\mathbf{r}, \mathbf{r}', \omega)\right]^{T}, \tag{S7}$$

where  $\epsilon(\mathbf{r},\omega)$  is the electric permittivity and  $\mu(\mathbf{r},\omega)$  is the magnetic permeability. As we consider a 2D periodic photonic structure, these two quantities fulfill the periodicity conditions  $\epsilon(\mathbf{r}+\mathbf{R},\omega)=\epsilon(\mathbf{r},\omega)$  and  $\mu(\mathbf{r}+\mathbf{R},\omega)=\mu(\mathbf{r},\omega)$ , with  $\mathbf{R}$  being an arbitrary lattice vector. These properties translate into an analogous periodicity condition for the Green tensor:

$$\mathbf{G}(\mathbf{r} + \mathbf{R}, \mathbf{r}' + \mathbf{R}, \omega) = \mathbf{G}(\mathbf{r}, \mathbf{r}', \omega). \tag{S8}$$

Within this quantization scheme, the total Hamiltonian of our periodic photoninc structure coupled to the emitter array is written as

$$\hat{H} = \hat{H}_e + \sum_{p=e,m} \int_0^\infty d\omega \int d^3r \, \hbar\omega \, \hat{\mathbf{f}}_p^{\dagger} (\mathbf{r}, \omega) \cdot \hat{\mathbf{f}}_p (\mathbf{r}, \omega) - \sum_i \sum_{h=1}^{N_E} \hat{\mathbf{d}}_i^{(h)} \cdot \hat{\mathbf{E}}(\mathbf{r}_i^{(h)}), \tag{S9}$$

where  $\hat{H}_e$  is the Hamiltonian of the 2D-periodic array of emitters and  $\hat{\mathbf{d}}_i^{(h)} = \hat{d}_i^{(h)} \mathbf{n}^{(h)}$  is the dipole operator of the multilevel emitter h in the unit cell i, located at  $\mathbf{r}_i^{(h)} = \mathbf{r}_0^{(h)} + \mathbf{R}_i$ ,  $\mathbf{r}_0^{(h)}$  being the position of the emitter in the reference unit cell. Note that we consider a single orientation  $\mathbf{n}^{(h)}$  per emitter and did not perform the two-level approximation here.

The periodic symmetry of the system implies that Bloch's theorem holds and, as shown in the following, that the full problem can be reduced to a problem restricted to the reciprocal unit cell.

To do so, we define the spin-wave basis for the emitter degrees of freedom

$$\hat{d}_{\mathbf{k}_{\parallel}}^{(h)} = \sum_{i} \hat{d}_{i}^{(h)} e^{-i\mathbf{k}_{\parallel} \cdot \mathbf{r}_{i}^{(h)}}, \tag{S10a}$$

$$\hat{d}_i^{(h)} = \frac{1}{V_B} \int_{V_B} d^2 k_{\parallel} \, \hat{d}_{\mathbf{k}_{\parallel}}^{(h)} e^{i\mathbf{k}_{\parallel} \cdot \mathbf{r}_i^{(h)}}.$$
 (S10b)

In addition, defining a reciprocal-space analogue of emitter-centered modes [2, 3]

$$\hat{B}_{\mathbf{k}_{\parallel}}^{(h)}(\omega) = \frac{1}{\hbar} \sum_{i} e^{-i\mathbf{k}_{\parallel} \cdot \mathbf{r}_{i}^{(h)}} \sum_{p} \int d^{3}r \, \mathbf{n}^{(h)} \cdot \mathbf{G}_{p}(\mathbf{r}_{i}^{(h)}, \mathbf{r}, \omega) \cdot \hat{\mathbf{f}}(\mathbf{r}, \omega), \tag{S11}$$

we find that the interaction Hamiltonian reads

$$\hat{H}_I = -\frac{\hbar}{V_B} \int_0^\infty d\omega \int_{V_B} d^2k_{\parallel} \sum_{\mathbf{h}} \hat{d}_{\mathbf{k}_{\parallel}}^{(\mathbf{h})\dagger} \hat{B}_{\mathbf{k}_{\parallel}}^{(\mathbf{h})}(\omega) + \text{h.c.}$$
 (S12)

The commutation relations

$$\left[\hat{B}_{\mathbf{k}_{\parallel}}^{(h)}(\omega), \hat{B}_{\mathbf{k}_{\parallel}'}^{(h')\dagger}(\omega')\right] = V_{B}\mathcal{G}_{h,h'}(\mathbf{k}_{\parallel},\omega)\delta(\omega-\omega')\delta(\mathbf{k}_{\parallel}-\mathbf{k}_{\parallel}'), \tag{S13}$$

determine the reciprocal-space spectral density that fully describes the light-matter coupling (see Eq. (\$20)):

$$\mathcal{G}_{h,h'}(\mathbf{k}_{\parallel},\omega) = \frac{\mu_0 \omega^2}{\pi \hbar} e^{-i\mathbf{k}_{\parallel}(r_0^{(h)} - r_0^{(h')})} \mathbf{n}^{(h)} \cdot \left[ \sum_i e^{i\mathbf{k}_{\parallel} \cdot \mathbf{R}_i} \operatorname{Im} \mathbf{G}(\mathbf{r}_0^{(h)}, \mathbf{r}_0^{(h')} + \mathbf{R}_i, \omega) \right] \cdot \mathbf{n}^{(h')}.$$
(S14)

In the derivation, we have used the important relation [1, 4]

$$\sum_{p} \int d^{3}s \,\mathbf{G}_{p}(\mathbf{r}, \mathbf{s}, \omega) \cdot \mathbf{G}_{p}^{\dagger}(\mathbf{r}', \mathbf{s}, \omega) = \frac{\hbar \mu_{0} \omega^{2}}{\pi} \operatorname{Im} \mathbf{G}(\mathbf{r}, \mathbf{r}', \omega), \tag{S15}$$

as well as the periodicity condition in Eq. (S8) and the completeness condition for plane waves  $\sum_i e^{i(\mathbf{k}_{\parallel} - \mathbf{k}'_{\parallel}) \cdot \mathbf{R}_i} = V_B \delta(\mathbf{k}_{\parallel} - \mathbf{k}'_{\parallel})$ . By comparing the reciprocal-space spectral density in Eq. (S14) to its real-space analogue [5], we find that the imaginary part of the dyadic Green tensor found in the latter is replaced by the lattice sum of the imaginary part of the dyadic Green tensor in the former. Furthermore, note that the diagonal elements of  $\mathcal{G}(\mathbf{k}_{\parallel},\omega)$  are equal to the conventional single-transition spectral density  $\mathbf{J}(\mathbf{k}_{\parallel},\omega)$  given in the main text up to the square of the transition dipole moment,  $d_h^2 \mathcal{G}_{h,h} = J_{h,h}$ . The same argument is true for the cross terms,  $d_h d_{h'} \mathcal{G}_{h,h'} = J_{h,h'}$ .

moment,  $d_h^2 \mathcal{G}_{h,h} = J_{h,h}$ . The same argument is true for the cross terms,  $d_h d_{h'} \mathcal{G}_{h,h'} = J_{h,h'}$ . Further insight into Eq (S14) can be provided by recalling the definition of the Bloch-periodic Green tensor,  $\mathcal{G}(\mathbf{k}_{\parallel},\mathbf{r},\mathbf{r}',\omega) = \sum_i \mathrm{e}^{\mathrm{i}\mathbf{k}_{\parallel}\cdot\mathbf{R}_i} \mathbf{G}(\mathbf{r},\mathbf{r}'+\mathbf{R}_i,\omega)$ , which is the solution of Maxwell's equations with Bloch-periodic boundary conditions. Equation (S8) implies that Bloch's theorem is fulfilled such that  $\mathcal{G}(\mathbf{k}_{\parallel},\mathbf{r}+\mathbf{R}_i,\mathbf{r}',\omega) = \mathrm{e}^{\mathrm{i}\mathbf{k}_{\parallel}\cdot\mathbf{R}_i}\mathcal{G}(\mathbf{k}_{\parallel},\mathbf{r},\mathbf{r}',\omega)$ . We can then use the Bloch-periodic Green tensor and Eq. (S8) to find that the anti-Hermitian part of the Bloch-periodic Green tensor reads

$$\mathcal{G}_{AH}(\mathbf{k}_{\parallel}, \mathbf{r}_{0}^{(h)}, \mathbf{r}_{0}^{(h')}, \omega) \equiv \frac{1}{2i} \left[ \mathcal{G}(\mathbf{k}_{\parallel}, \mathbf{r}_{0}^{(h)}, \mathbf{r}_{0}^{(h')}, \omega) - \mathcal{G}^{\dagger}(\mathbf{k}_{\parallel}, \mathbf{r}_{0}^{(h')}, \mathbf{r}_{0}^{(h)}, \omega) \right]$$
(S16)

$$= \sum_{i} e^{i\mathbf{k}_{\parallel} \cdot \mathbf{R}_{i}} \operatorname{Im} \mathbf{G}(\mathbf{r}_{0}^{(h)}, \mathbf{r}_{0}^{(h')} + \mathbf{R}_{i}, \omega), \tag{S17}$$

such that Eq. (S14) reduces to Eq. (1) of the main text.

The next step is to perform an orthogonalization transformation  $\hat{B}^{(h)}_{\mathbf{k}_{\parallel}}(\omega) = \sum_{h'} W_{h,h'}(\mathbf{k}_{\parallel},\omega) \hat{a}^{(h')}_{\mathbf{k}_{\parallel}}(\omega)$  such that  $\left[\hat{a}^{(h)}_{\mathbf{k}_{\parallel}}(\omega),\hat{a}^{(h')\dagger}_{\mathbf{k}'_{\parallel}}(\omega')\right] = V_{B}\delta_{hh'}\delta(\mathbf{k}_{\parallel}-\mathbf{k}'_{\parallel})\delta(\omega-\omega')$ , where  $\mathbf{W}\cdot\mathbf{W}^{\dagger}=\mathcal{G}$  [6]. The interaction Hamiltonian then reads

$$H_{I} = -\frac{\hbar}{V_{B}} \int_{V_{B}} d^{2}k_{\parallel} \int_{0}^{\infty} d\omega \sum_{h,h'} \left[ \hat{d}_{\mathbf{k}_{\parallel}}^{(h)\dagger} W_{h,h'}(\mathbf{k}_{\parallel},\omega) \hat{a}_{\mathbf{k}_{\parallel}}^{(h')}(\omega) + \text{h.c.} \right].$$
 (S18)

The total Hamiltonian can be finally written in terms of the momentum resolved Hamiltonian  $\hat{H}_{\mathbf{k}_{\parallel}}$ :

$$\hat{H} = \frac{1}{V_B} \int_{V_B} d^2 k_{\parallel} \hat{H}_{\mathbf{k}_{\parallel}},\tag{S19}$$

with:

$$\hat{H}_{\mathbf{k}_{\parallel}} = \hat{H}_{e,\mathbf{k}_{\parallel}} + \int_{0}^{\infty} d\omega \sum_{h} \hbar\omega \, \hat{a}_{\mathbf{k}_{\parallel}}^{(h)\dagger}(\omega) \hat{a}_{\mathbf{k}_{\parallel}}^{(h)}(\omega) - \int_{0}^{\infty} d\omega \sum_{h,h'} \left[ \hat{d}_{\mathbf{k}_{\parallel}}^{(h)\dagger} \hbar W_{h,h'}(\mathbf{k}_{\parallel},\omega) \hat{a}_{\mathbf{k}_{\parallel}}^{(h')}(\omega) + \text{h.c.} \right]. \tag{S20}$$

To find the reciprocal-space spectral density for the configuration considered in the main text, we used the T-matrix-based scattering code treams [7].

From now on, we set  $\hbar = 1$ .

### SII. LASER DRIVING

In the framework of macroscopic quantum electrodynamics, coherent laser driving in the present of absorptive and lossy environments can be included straightforwardly [2, 8]. Formally, the emitters and field modes are driven by the laser. One can analytically remove the driving of the field modes, by replacing the driving field of the emitters by the structure-enhanced field at the position of the hth emitter in the unit cell  $\mathbf{E}_h$ , i.e. by the field obtained by propagating the incoming laser field to the location of the emitter  $\mathbf{r}_0^{(h)}$  in the presence of the electromagnetic environment (here the metasurface).

In the manuscript, we consider single-mode plane wave driving with frequency  $\omega_{\rm L}$  and in-plane wave-vector  ${\bf k}_{\rm L}$  and find  $\mathbf{E}_h = \widetilde{\mathbf{E}}_h \mathrm{e}^{-\mathrm{i}\mathbf{k}_L \cdot \mathbf{r}_0^{(h)}}$  numerically again using the T-matrix-based scattering code treams [7]. The corresponding driving term in the Hamiltonian then reads

$$\hat{H}_{L} = \sum_{h} \Omega_{h} (\hat{\sigma}_{\mathbf{k}_{L}}^{(h)\dagger} + \hat{\sigma}_{\mathbf{k}_{L}}^{(h)}), \tag{S21}$$

where the Rabi frequency of the laser drive reads  $\Omega_h = \mathbf{d}_h \cdot \mathbf{E}_h$ .

## SIII. HOLSTEIN-PRIMAKOFF TRANSFORMATION AND SQUEEZING HAMILTONIAN

In general, the equations of motion at fixed in-plane momentum of the few-mode model

$$\dot{\hat{\rho}}_{\mathbf{k}_{\parallel}} = -\mathrm{i}[\hat{H}_{\mathbf{k}_{\parallel}}, \hat{\rho}_{\mathbf{k}_{\parallel}}] + \sum_{i} \kappa_{\mathbf{k}_{\parallel}, i} L_{\hat{a}_{\mathbf{k}_{\parallel}, i}}[\hat{\rho}_{\mathbf{k}_{\parallel}}], \tag{S22}$$

with  $L_{\hat{O}}[\hat{\rho}] = \hat{O}\hat{\rho}\hat{O}^{\dagger} - \frac{1}{2}\{\hat{O}^{\dagger}\hat{O},\hat{\rho}\}$ , are not closed, since spin-wave excitations with different in-plane momenta do not commute, that is,  $[\sigma_{\mathbf{k}_{\parallel}}^{(h)}, \sigma_{\mathbf{k}_{\parallel}'}^{(h)\dagger}] \neq 0$  for  $\mathbf{k}_{\parallel} \neq \mathbf{k}_{\parallel}'$ . In this section, we simplify the equations of motion of the few-mode model by systematically performing a low-excitation approximation via a Holstein-Primakoff transformation [9]:

$$\hat{\sigma}_i = \sqrt{1 - \hat{b}_i^{\dagger} \hat{b}_i} \hat{b}_i. \tag{S23}$$

Here,  $\hat{b}_i$  are bosonic annihilation operators and note that, for simplicity, here we only consider the case of a single emitter per unit cell with  $\hat{\sigma}_{\mathbf{k}_{\parallel}}^{(1)} = \hat{\sigma}_{\mathbf{k}_{\parallel}}$ .

### Linear approximation, stead-state, and field seen by the emitter

In the low-excitation regime, we find  $\langle \hat{b}_i^{\dagger} \hat{b}_i \rangle \ll 1$  such that we can expand Eq. (S23) to lowest order, finding  $\hat{\sigma}_i \approx \hat{b}_i$ . In reciprocal space, this reads  $\hat{\sigma}_{\mathbf{k}_{\parallel}}\approx\hat{b}_{\mathbf{k}_{\parallel}}$  with

$$\hat{b}_{\mathbf{k}_{\parallel}} = \sum_{i} \hat{b}_{i} e^{-i\mathbf{k}_{\parallel} \cdot \mathbf{r}_{i}},\tag{S24}$$

where

$$[\hat{b}_{\mathbf{k}_{\parallel}}, \hat{b}_{\mathbf{k}_{\parallel'}}^{\dagger}] = V_B \delta(\mathbf{k}_{\parallel} - \mathbf{k}_{\parallel}'). \tag{S25}$$

As a result, we find the linearized few-mode Hamiltonian

$$\hat{H}_{\mathbf{k}_{\parallel},\text{lin}} = \omega_{\mathrm{E}} \hat{b}_{\mathbf{k}_{\parallel}}^{\dagger} \hat{b}_{\mathbf{k}_{\parallel}} + \sum_{ij} \omega_{\mathbf{k}_{\parallel},ij} \hat{a}_{\mathbf{k}_{\parallel},i} \hat{a}_{\mathbf{k}_{\parallel},j} + \sum_{i} (g_{\mathbf{k}_{\parallel},i} \hat{b}_{\mathbf{k}_{\parallel}}^{\dagger} \hat{a}_{\mathbf{k}_{\parallel},i} + \text{h.c.}), \tag{S26}$$

which conserves the in-plane momentum, such that we can diagonalize it for each  $\mathbf{k}_{\parallel}$  individually. This gives the polaritonic modes shown in Fig. 3(b) in the main text. Furthermore, we add a laser driving term  $\hat{H}_{\rm L} = \Omega(\hat{b}_{\bf k_{\rm L}}^{\dagger} + \hat{b}_{\bf k_{\rm L}})$ , compare Section SII, such that the Hamiltonian in the co-rotating frame and in the linear approximation at the laser in-plane momentum reads

$$\hat{H}_{\mathbf{k}_{\mathrm{L}},\mathrm{lin}} = (\omega_{\mathrm{E}} - \omega_{\mathrm{L}})\hat{b}_{\mathbf{k}_{\mathrm{L}}}^{\dagger}\hat{b}_{\mathbf{k}_{\mathrm{L}}} + \hat{H}_{\mathrm{L}} + \sum_{ij} (\omega_{\mathbf{k}_{\mathrm{L}},ij} - \omega_{\mathrm{L}}\delta_{ij})\hat{a}_{\mathbf{k}_{\mathrm{L}},i}^{\dagger}\hat{a}_{\mathbf{k}_{\mathrm{L}},j} + \sum_{i} (g_{\mathbf{k}_{\mathrm{L}},i}\hat{b}_{\mathbf{k}_{\mathrm{L}}}^{\dagger}\hat{a}_{\mathbf{k}_{\mathrm{L}},i} + \mathrm{h.c.}). \tag{S27}$$

This reduces the equations of motion of the emitters and field modes at the laser in-plane momentum to those of two coupled driven lossy harmonic oscillators, for which we can find steady-state solutions analytically [10]. The steady-state solutions for the driven emitter and field operators read  $\hat{b}_{\mathbf{k}_{\mathrm{L}},\mathrm{ss}} = b_{\mathbf{k}_{\mathrm{L}}} + \hat{b}_{\mathbf{k}_{\mathrm{L}}}$  and  $\hat{a}_{\mathbf{k}_{\mathrm{L}},i,\mathrm{ss}} = a_{\mathbf{k}_{\mathrm{L}},i} + \hat{a}_{\mathbf{k}_{\mathrm{L}},i}$ , respectively, with their coherent amplitudes given by

$$\mathcal{A}_{\mathbf{k}_{L}} = -\mathbf{H}_{\text{eff}}^{-1} \cdot \mathbf{\Omega}. \tag{S28}$$

 $\mathcal{A}_{\mathbf{k}_{\mathrm{L}}} = -\mathbf{H}_{\mathrm{eff}}^{-1} \cdot \mathbf{\Omega}. \tag{S28}$  Here,  $\mathcal{A}_{\mathbf{k}_{\mathrm{L}}} = (a_{0,\mathbf{k}_{\mathrm{L}}}, \ldots, a_{N_{M},\mathbf{k}_{\mathrm{L}}}, \theta_{\mathbf{k}_{\mathrm{L}}}), \mathbf{\Omega} = (0, \ldots, 0, \Omega), N_{\mathrm{M}}$  is the number of modes, and the effective non-Hermitian matrix  $\mathbf{H}_{\mathbf{k}_{\mathrm{L}}} = \mathbf{n}_{\mathrm{L}}$ matrix  $H_{\mathrm{eff}}$  reads

$$\mathbf{H}_{\text{eff}} = \begin{pmatrix} \widetilde{\mathbf{h}}_{\mathbf{k}_{L}} & \mathbf{g}_{\mathbf{k}_{L}}^{*} \\ \mathbf{g}_{\mathbf{k}_{L}} & \omega_{E} - \omega_{L} \end{pmatrix}, \tag{S29}$$

with  $h_{\mathbf{k}_{\mathrm{L}},ij} = \omega_{\mathbf{k}_{\mathrm{L}},ij} - \omega_{\mathrm{L}}\delta_{ij} - \mathrm{i}\kappa_{\mathbf{k}_{\mathrm{L}},i}\delta_{ij}/2$ . Note that in the linear approximation, all other field and emitter operators with  $\mathbf{k}_{\parallel} \neq \mathbf{k}_{\mathrm{L}}$  remain in the ground state.

In the linear approximation, the field seen by the emitter is given by  $E_{\text{loc}} = \Omega + \sum_i g_{\mathbf{k}_{\text{L}},i} a_{\mathbf{k}_{\text{L}},i}$ , which is shown for the case of the dielectric emitter array in Fig. 3(b) of the main text.

#### **B.** Nonlinear interaction

To account for the nonlinearity of the two-level emitter, we consider the resummation [11] of the Holstein-Primakoff expansion (S23) which is exact for single spins considered here, by setting

$$\hat{\sigma}_i \approx \left(1 - \hat{b}_i^{\dagger} \hat{b}_i\right) \hat{b}_i. \tag{S30}$$

In reciprocal space, we find

$$\hat{\sigma}_{\mathbf{k}_{\parallel}} = \hat{b}_{\mathbf{k}_{\parallel}} - \frac{1}{V_{B}^{2}} \int_{V_{B}} d^{2}k_{\parallel}' \int_{V_{B}} d^{2}k_{\parallel}'' \, \hat{b}_{\mathbf{k}_{\parallel}''} \hat{b}_{\mathbf{k}_{\parallel}''} \hat{b}_{\mathbf{k}_{\parallel} + \mathbf{k}_{\parallel}' - \mathbf{k}_{\parallel}''}. \tag{S31}$$

Assuming that the coherent displacement  $\mathcal{A}_{\mathbf{k}_L}$  of the field and emitter modes at  $\mathbf{k}_L$  is much stronger than the populations of any other state with  $\mathbf{k}_{\parallel} \neq \mathbf{k}_L$ , we find the following two additional nonlinear contributions to the linear Hamiltonian (S26) considered in the previous section: A squeezing-type interaction

$$\hat{H}_{\mathrm{sq},\mathbf{k}_{\parallel}} = \sum_{i} g_{\mathbf{k}_{\parallel},i}^{*} \mathcal{B}_{\mathbf{k}_{\perp}}^{2} \hat{a}_{\mathbf{k}_{\parallel},i}^{\dagger} \hat{b}_{\overline{\mathbf{k}}_{\parallel}}^{\dagger} + E_{\mathrm{loc}} \mathcal{B}_{\mathbf{k}_{\perp}} \hat{b}_{\mathbf{k}_{\parallel}}^{\dagger} \hat{b}_{\overline{\mathbf{k}}_{\parallel}}^{\dagger} + (\mathbf{k}_{\parallel} \leftrightarrow \overline{\mathbf{k}}_{\parallel})] + \text{h.c.}, \tag{S32}$$

and a beam-splitter-type interaction

$$\hat{H}_{\mathrm{bs},\mathbf{k}_{\parallel}} = \sum_{i} g_{\mathbf{k}_{\parallel},i}^{*} |\delta_{\mathbf{k}_{\perp}}|^{2} \hat{a}_{\mathbf{k}_{\parallel},i}^{\dagger} \hat{b}_{\overline{\mathbf{k}}_{\parallel}} + E_{\mathrm{loc}} \delta_{\mathbf{k}_{\perp}}^{*} \hat{b}_{\mathbf{k}_{\parallel}}^{\dagger} \hat{b}_{\overline{\mathbf{k}}_{\parallel}} + (\mathbf{k}_{\parallel} \leftrightarrow \overline{\mathbf{k}}_{\parallel})] + \text{h.c.}$$
(S33)

Here,  $(\mathbf{k}_{\parallel} \leftrightarrow \overline{\mathbf{k}}_{\parallel})$  denotes adding the preceding terms subject to the replacement  $\mathbf{k}_{\parallel} \leftrightarrow \overline{\mathbf{k}}_{\parallel}$ .  $\hat{H}_{\mathrm{sq},\mathbf{k}_{\parallel}}$  denotes a multimode squeezing Hamiltonian also given in the main text that describes processes in which two excitations of the coherently displaced modes or emitters generate or annihilate pairs of entangled excitations with opposite (but potential finite) in-plane wave-vector  $\mathbf{k}_{\parallel}$ . The beam-splitter Hamiltonian leads to a shift in the polaritonic frequencies but is of minor importance in our discussion of nonlinear light generation here.

Figure 4 of the main text has been obtained by first finding steady-state solutions  $\theta_{\mathbf{k}_L}$  and  $a_{\mathbf{k}_L,i}$  of the equations of motion given by the linear parts of the Hamiltonian at the laser frequency and the additional Lindblad terms, as given by Eq. (S22) and Eq. (S27). Subsequently,  $\theta_{\mathbf{k}_L}$  and  $a_{\mathbf{k}_L,i}$  are used as input for the non-linear Hamiltonian of modes with  $\mathbf{k}_{\parallel} \neq \mathbf{k}_L$  in Eqs. (S32) and (S33). The steady-state populations of these modes in the presence of the linear and nonlinear Hamiltonian as well as the Linblad term were then numerically calculated to obtain  $\gamma_{\mathbf{k}_{\parallel}}$  given by

$$\gamma_{\mathbf{k}_{\parallel}} = \sum_{i,j} (\kappa_{\mathbf{k}_{\parallel},i} + \kappa_{\overline{\mathbf{k}}_{\parallel},j}) \left\langle \hat{a}_{\mathbf{k}_{\parallel},i}^{\dagger} \hat{a}_{\overline{\mathbf{k}}_{\parallel},j}^{\dagger} \hat{a}_{\mathbf{k}_{\parallel},i} \hat{a}_{\overline{\mathbf{k}}_{\parallel},j} \right\rangle_{\mathrm{ss}}.$$
 (S34)

- \* johannes.feist@uam.es
- † fj.garcia@uam.es
- [1] S. Scheel and S. Buhmann, Acta Phys. Slovaca 58, 675 (2008).
- [2] J. Feist, A. I. Fernández-Domínguez, and F. J. García-Vidal, Nanophotonics 10, 477 (2020).
- [3] S. Y. Buhmann and D.-G. Welsch, Phys. Rev. A 77, 012110 (2008).
- [4] S. Y. Buhmann, *Dispersion forces I* (Springer, Berlin, 2012).
- [5] I. Medina, F. J. García-Vidal, A. I. Fernández-Domínguez, and J. Feist, Phys. Rev. Lett. 126, 093601 (2021).
- [6] M. Sánchez-Barquilla, F. J. García-Vidal, A. I. Fernández-Domínguez, and J. Feist, Nanophotonics 11, 4363 (2022).
- [7] D. Beutel, I. Fernandez-Corbaton, and C. Rockstuhl, Comput. Phys. Commun. 297, 109076 (2024).
- [8] F. Lindel, R. Bennett, and S. Y. Buhmann, Phys. Rev. A 103, 033705 (2021).
- [9] T. Holstein and H. Primakoff, Phys. Rev. 58, 1098 (1940).
- [10] M. O. Scully and M. S. Zubairy, Quantum optics (Cambridge University Press, Cambridge, 1997).
- [11] M. Vogl, P. Laurell, H. Zhang, S. Okamoto, and G. A. Fiete, Phys. Rev. Res. 2, 043243 (2020).